

Structure and dynamics of magnetorheological fluids in rotating magnetic fields

Sonia Melle* and Gerald G. Fuller

Department of Chemical Engineering, Stanford University, Stanford, California 94305-5025

Miguel A. Rubio

Departamento de Física Fundamental, UNED, Paseo Senda del Rey 9, Madrid 28040, Spain

(Received 22 October 1999)

We report on the orientation dynamics and aggregation processes of magnetorheological fluids subject to rotating magnetic fields using the technique of scattering dichroism. In the presence of stationary fields we find that the mean length of the field-induced aggregates reaches a saturation value due to finite-size effects. When a rotating field is imposed, we see the chains rotate with the magnetic field frequency (synchronous regime) but with a retarded phase angle for all the rotational frequencies applied. However, two different behaviors are found below or above a critical frequency f_c . Within the first regime (low frequency values) the size of the aggregates remains almost constant, while at high frequencies this size becomes shorter due to hydrodynamic drag. Experimental results have been reproduced by a simple model considering a torque balance on the chainlike aggregates.

PACS number(s): 83.80.Gv, 75.50.Mm, 82.70.Dd, 45.50.-j

I. INTRODUCTION

Magnetic fluids subjected to uniaxial magnetic fields become optically anisotropic due to the orientation of stringlike aggregates of the colloidal particles making up the suspensions [1]. Indeed, optical techniques including video microscopy, light transmission, and light scattering have been used to characterize the kinetics of field-induced structures formation in magnetorheological (MR) fluids [2–9]. When an electrorheological (ER) or MR fluid is subjected to steady or oscillatory shear, hydrodynamic forces will induce both structure orientation and size changes. This behavior has been theoretically predicted by a simple model considering the balance between hydrodynamic and electrostatic or magnetostatic forces [10,11].

Polarizable systems consisting of many elongated objects exhibit interesting dynamic behaviors when subjected to a rotating electric or magnetic field. Similar regimes depending on the angular velocity of the field are found for mesomorphic molecules in a nematic liquid crystal [12], for macroscopic cylindrical objects made of phospholipidic bilayers [13], and for magnetic liquid microdroplets [14]. The director axis of the structure rotates synchronously with the field at low rotational frequencies and up to a threshold value. Above the threshold, the rotation of the director is no longer synchronous with the field, and its time-average rotation rate is less than the angular velocity of the field, leading to an asynchronous regime. In the high frequency asynchronous regime, the objects follow a so-called “jerky” motion [15], consisting of a rotation with stops and backward motions. In this paper we report on the structural evolution of MR fluids under the application of stationary and spatially rotating magnetic fields by means of scattering dichroism. We will

analyze the different dynamical regimes that appear in this system.

When a unidirectional magnetic field \vec{H} is applied to a suspension, the field induces a magnetic dipolar moment in the magnetic particles \vec{m} . For low magnetic fields (typically less than 25 kA/m), the particles used in this study have a paramagnetic behavior $\vec{m} = (4/3)\pi a^3 \chi_{eff} \vec{H}$, with a the particle radius and $\chi_{eff} = 3(\mu_p - \mu_s) / (\mu_p + 2\mu_s)$ its effective magnetic susceptibility. Here μ_p and μ_s are the permeability of the particles and the solvent, respectively [16]. A key dimensionless parameter to characterize the formation of chains is the ratio between the magnetic and thermal energies, $\lambda = (\pi \mu_0 a^3 \chi_{eff}^2 H^2) / (9 k_B T)$, where μ_0 is the vacuum magnetic permeability, k_B the Boltzmann constant, and T the temperature. Therefore, for the range of fields measured here [$1.2 < H(kA/m) < 25$] we obtain $15 < \lambda < 6250$ at room temperature, so the magnetic interaction will dominate over Brownian thermal motion. Because these chains have a preferred orientation, the suspension exhibits an optical anisotropy as reflected in a complex refractive index tensor, $\hat{n}_{ij} = n'_{ij} - i n''_{ij}$, due to the polarization dependent scattering from oriented aggregates. Furthermore, as the length scale of the scattering objects encountered in these measurements is comparable to the wavelength of the light, the dichroism $\Delta n''$ (the anisotropy of the imaginary part) will be larger than the birefringence $\Delta n'$ (the anisotropy of the real part) [17].

Using Rayleigh-Debye theory for the scattering of light, the following expression can be used to estimate the scattering dichroism in the forward direction generated from a set of n_c chains per unit volume, assuming that the chains are long circular cylinders of length L and radius R [17]:

$$\Delta n'' = \frac{2n_c L}{k^2} (\text{Re}[T_2(\theta_{scat}=0)] - \text{Re}[T_1(\theta_{scat}=0)]). \quad (1.1)$$

Here $k = 2\pi/\lambda_l$ is the wave vector of the laser beam, and

*Permanent address: Departamento de Física Fundamental, UNED, Paseo Senda del Rey 9, Madrid 28040, Spain.

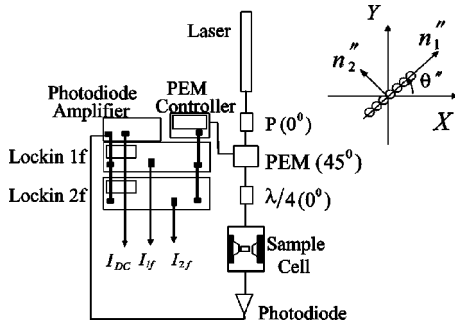


FIG. 1. Schematic diagram of the linear dichroism optical train. The absorption of the incident light is different in the parallel direction than in the perpendicular direction to the long axis of the aggregates. The dichroism determines the difference between both components, $\Delta n'' = n''_1 - n''_2$. This setup enables one to measure the orientation angle of the structures θ'' , which is the angle between the reference axis of the optical train and the long axis of the aggregates.

$T_i(\theta_{scat}=0)$ is a function of k , R , and the isotropic refractive indexes of solvent and particles. From Eq. (1.1) we deduce the dichroism is related to the number of particles forming the aggregates per unit volume given by $n_p = (n_c L)/(2R)$.

II. EXPERIMENTAL METHODS AND MATERIALS

A. Scattering dichroism setup

A schematic of the optical train used to measure linear dichroism is shown in Fig. 1. Monochromatic light produced by a He-Ne laser ($\lambda_l = 632.8$ nm) is sent through a polarizer oriented at 0° (reference angle of the optical system), a photoelastic modulator (PEM) at 45° and a quarter wave plate at 0° . The PEM produces a time dependent retardation given by $\delta'_{PEM} = A \sin(2\pi f_{PEM} t)$, where A is the amplitude, and $f_{PEM} = 50$ kHz is the frequency. The light is then passed through the sample and the transmitted light is detected by a photodiode. The signal from the photodiode is then sent to two phase lock-in amplifiers, one of which extracts the signal component at the frequency of the PEM (I_{1f}) and the other which extracts the signal component at the second harmonic (I_{2f}). The dc component of the light is isolated by passing the transmitted beam through a high pass filter. The three voltages (I_{dc} , I_{1f} , and I_{2f}) are then digitized and measured using a 16-bit analog-to-digital data acquisition device (National Instruments). With this optical train we can simultaneously calculate the dichroism $\Delta n'' = n''_1 - n''_2$ and the orientation angle θ'' (see Fig. 1) [18,19].

B. Sample cell

The fluid sample is sandwiched between two circular quartz windows held in place by a Delrin attachment (external dimensions $13 \times 13 \times 6$ mm³) designed to prevent evaporation of the solvent (see Fig. 2). The inner diameter dimensions of the cell are 6.5 mm, and the thickness is set by different spacers. The optical measurements are taken at an area in the cell that corresponds to the diameter of the laser (3 mm). The sample is surrounded by two orthogonal pairs of magnetic coils. These coils are housed in a temperature

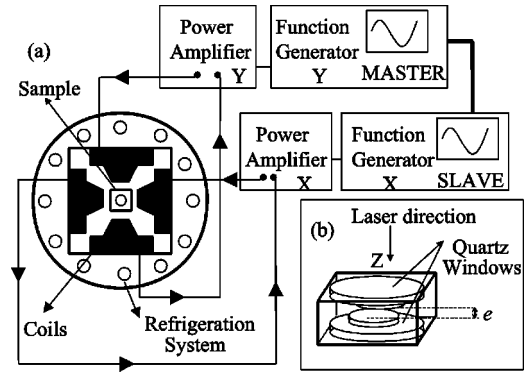


FIG. 2. (a) Sketch of the coils system from the direction of the laser beam to produce a rotating magnetic field in the sample. (b) Details of a quartz cell filled with MR fluid.

controlled aluminum cylinder to prevent heating effects. As four coils cannot be in a Helmholtz configuration because of geometrical constraints, we have optimized their relative positions and shapes using a numerical simulation to obtain a magnetic field as homogeneous as possible throughout the sample. This is necessary to prevent local changes of concentration due to the transport of the magnetic latex particles under the effect of field gradients. Experimentally we can achieve magnetic fields on the order of 25 kA/m with a variation less than 3% in the vicinity of the sample. All experiments were performed at room temperature, which ranged from 20 to 22 °C.

C. Magnetic suspensions

We used two different magnetic suspensions manufactured by *Rhône Poulenc* formed of magnetic latex microspheres, which contain the same small ferromagnetic particles as those dispersed in a ferrofluid. These aqueous dispersions have a solid content of 10%. Magnetite crystals (Fe_2O_3) of diameter between 1 and 20 nm are dispersed in styrene (S) or divinylbenzene (DVB) monomers and polymerized using a suspension process yielding magnetite-laden S/DVB-based spheres with mean diameter around 1 μm . The surface of these microspheres is composed of carboxylic acid (-COOH) groups with an added surfactant coating layer of sodium dodecyl sulfate (SDS) to stabilize the dispersions. Since these small magnets are randomly oriented inside these microparticles, the resulting magnetic moment is zero in the absence of an external magnetic field. Under sufficiently low magnetic fields these particles exhibit superparamagnetic behavior with virtually no hysteresis or magnetic remanence as a result of the orientation of the extremely small magnetite grains dispersed in the polymer matrix. Due to their small average diameters the sedimentation time is long enough to neglect gravitational effects. In Table I, we list the properties of the two particles that were used.

For the uniaxial magnetic field experiments we used the Estapor magnetic latex solution M1-180/20 with a sample thickness of $e = 130$ μm , while for the dynamic experiments employing spatially rotating magnetic fields we diluted the concentrated solution M1-180/12 in glycerol to achieve a solvent volume concentration of 82.5% glycerol. The dilution in glycerol reduced the SDS concentration, and additional SDS was added to achieve a concentration equal to the

TABLE I. Properties of the two particles that were used.

Magnetic latex microspheres solution	M1-180/20	M1-181/2
Mean diameter	0.87 μm	1.01 μm
Magnetic content	24.8%	13%
Polymer nature	PDVB	PS
Surface group content	53 $\mu\text{eq/g}$	20 $\mu\text{eq/g}$
Effective magnetic susceptibility	1.65	0.96
Density	1.38 g/cm^3	1.174 g/cm^3
Saturation	20 emu/g	12 emu/g

original solution (5 g/l). The final volume fraction of the M1-180/12 particles after dilution was $\phi_V=0.016$. The sample thickness in these experiments was $e=100 \mu\text{m}$. The viscosity of this new solution without applying an external magnetic field was measured using a Rheometrics Dynamic Analyzer RDA II to be $\eta=(0.975\pm 0.003)$ poises at 22 $^\circ\text{C}$.

III. EXPERIMENTAL RESULTS

Two different experiments were performed on the MR fluids by applying specified magnetic fields in the plane (X, Y) perpendicular to the optical path (axis Z). In the first experiment, a unidirectional pulse magnetic field was applied, while in the second one, a rotational magnetic field was applied. The pulsed magnetic field was achieved by using a square electric pulse function generator to one of the pairs of coils shown in Fig. 1. The rotating magnetic field was achieved by applying sinusoidal electric signals to the two orthogonal pairs of coils by means of two function generators referenced to one another at a phase difference of 90° (see Fig. 2). The function generators allowed for control of both the amplitude and frequency of the rotating magnetic field.

A. Transient/steady experiments in uniaxial fields

We have analyzed the temporal evolution of dichroism in response to square pulses of magnetic fields. Figure 3 shows the average of ten of these cycles for two different magnetic field strengths of 1.24 and 3.72 kA/m. In the absence of

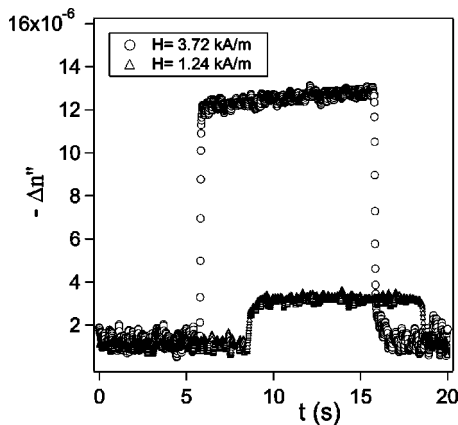


FIG. 3. Average signal of the temporal evolution of the dichroism in response to a square pulse of magnetic field for two different magnetic field strengths (1.24 and 3.72 kA/m). Each curve is averaged on ten cycles.

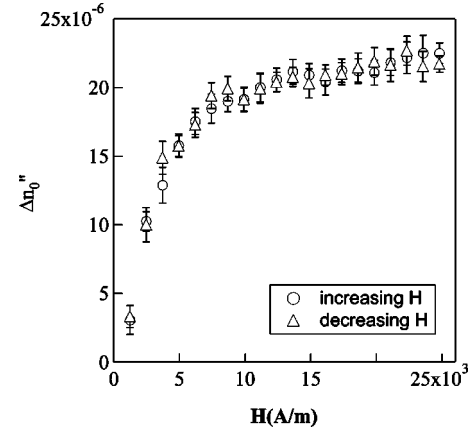


FIG. 4. Equilibrium value of the dichroism vs magnetic field intensity: (circles) increasing magnetic field and (triangles) decreasing magnetic field. Hysteresis is not present in our system.

magnetic field the dichroism is zero, corresponding to an isotropic medium. When a constant magnetic field is suddenly applied, the dichroism increases until an equilibrium value $\Delta n''_0$ is reached. The growth of the dichroism corresponds to the formation of chainlike structures aligned in the direction of the field due to magnetic dipolar interaction between the particles. The field pulse duration was chosen such that the equilibrium value of the dichroism was reached. In these experiments, the pulse width was $T_B=20$ sec and the sampling frequency was $f_s=100$ Hz. When the magnetic field is switched off, the dichroism decays to zero. In the absence of a magnetic field the relaxation process of the structures is governed solely by Brownian diffusion of the particles.

The dependence of the equilibrium value of the dichroism with the magnetic field intensity is shown in Fig. 4. As the magnetic field strength is increased, the equilibrium value of the dichroism increases. At a low magnetic field intensity the dichroism increases rapidly with increasing field intensity. However at higher magnetic fields, above approximately 8 kA/m, the dichroism reaches a plateau value of about $\Delta n''_0 \approx -20 \times 10^{-6}$. The results in Fig. 4 were obtained by both increasing and decreasing the magnetic field in order to detect evidence of hysteresis. The lack of hysteresis is consistent with the paramagnetic character of the particles. The fact that the dichroism increases with the magnetic field shows that the number of aggregated particles is increasing [see Eq. (1.1)], which is expected since the magnetic moment of the particles increases with the magnetic field. However, when the length of the chains exceeds the size of the laser beam, a saturation phenomenon for the induced dichroism takes place.

B. Dynamic experiments in rotating fields

As described previously, rotating magnetic fields in the plane (X, Y) perpendicular to the optical path direction (axis Z), $\vec{H}(t) = H \cos(\omega t)\vec{u}_x + H \sin(\omega t)\vec{u}_y$, were also applied to the suspensions. Under these conditions, two torques act on the aggregates: a magnetic torque Γ_m that rotates the chainlike structures due to dipolar interaction among the particles orientated in the direction of the magnetic field, and a hydro-

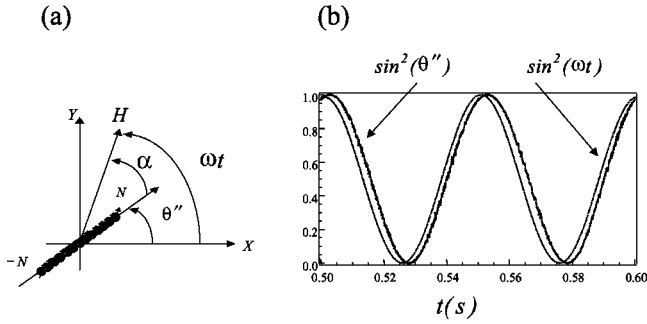


FIG. 5. (a) Definition of the phase lag between the magnetic field and the chains. (b) Temporal evolution of the magnetic field and aggregate direction. As an example we plot the experimental data for a field of 12.4 kA/m and $f = \omega/2\pi = 10$ Hz.

dynamic torque Γ_h arising from the rotational friction of the structures in the suspending fluid.

In order to study the structures induced by the rotating magnetic field we have simultaneously measured the time evolution of the dichroism and the orientation angle θ'' , i.e., the angle between the reference axis of the optical train and the long axis of the aggregates [see Fig. 5(a)]. By comparing θ'' with the temporal evolution of the magnetic field direction given by ωt we found, as can be observed in Fig. 5(b), that the structures follow the magnetic field rotating with the same frequency but with a phase lag independent of time for all frequencies measured. This fact has also been probed by means of power spectrum analysis for the experimental signals of $\sin^2(\omega t)$ and $\sin^2\theta''$. Therefore, we define the phase lag between the field and the aggregates as

$$\alpha(t) = \omega t - \theta''(t). \quad (3.1)$$

In Fig. 6 the dichroism generated by the suspension is plotted as a function of field strength for various frequencies of the rotating field. All the curves show a monotonic increase in dichroism to a plateau value, but with a strong dependence on the rotational frequency. This effect is shown more directly in Fig. 7, where the dichroism is plotted against magnetic field frequency ($f = \omega/2\pi$) in a log-log form. As the frequency of the applied field is increased, the dichroism is strongly reduced. This plot clearly shows two distinct re-

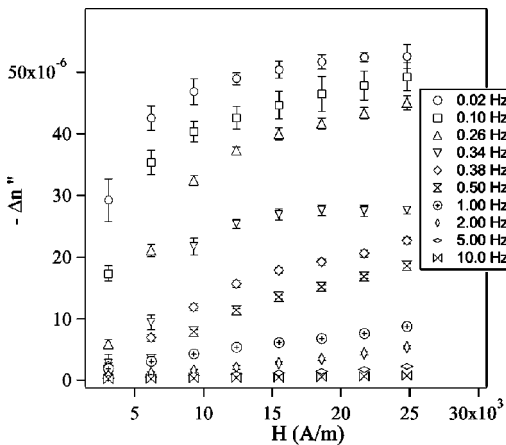


FIG. 6. Dichroism vs magnetic field intensity for frequencies ranging from 0.02 to 10 Hz.

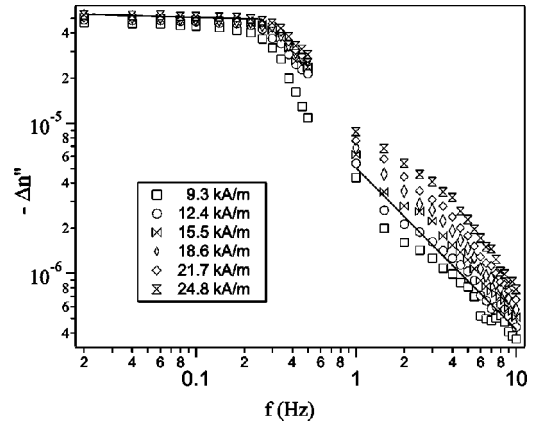


FIG. 7. Dichroism as a function of magnetic field frequency for a range of magnetic field strength (log-log plot).

gions for frequencies below and above a critical frequency f_c , near to 0.3 Hz. Below this critical frequency the dichroism is essentially independent of frequency, and the aggregate size remains almost constant. However, once this frequency is surpassed, the dichroism decreases with frequency, which reveals a diminution of the aggregate size. The critical frequency separating these two regions increases with the magnitude of the applied magnetic field. This behavior is expected, since the strength of the interparticle magnetic forces scales with the applied field. It is found above 1 Hz that the dichroism drops with frequency, with a scaling of approximately $\Delta n'' \approx f^{-1}$.

The phase difference α between the orientation of the chains and the magnetic field versus the field strength is plotted in Fig. 8 for different rotational frequencies. We see a diminution of the phase difference with increasing magnetic field intensity, as expected because the magnetic torque increases with the magnetic field strength. Analyzing experimental data for the variation of the phase difference α with the frequency of the magnetic field (see Fig. 9), we observe that this phase difference increases with frequency over the whole range of frequencies. However, as we found for the dichroism results (see Figs. 6 and 7), two different responses are seen depending on the frequency value. At low frequencies (below the critical frequency) the phase difference grows very quickly, while at high frequencies the increase of the phase difference is relatively slow.

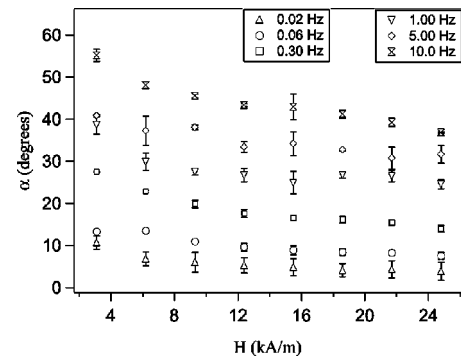


FIG. 8. Phase lag as a function of magnetic field intensity for frequencies ranging from 0.02 to 10 Hz.

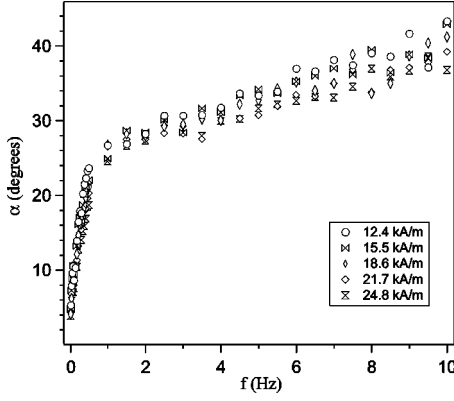


FIG. 9. Phase lag as a function of magnetic field frequency.

IV. THEORETICAL MODEL

To analyze the behavior of the phase lag, we developed a simple chain model where dipolar interactions and hydrodynamics forces dominate thermal forces. This model ignores chain-chain interaction. Consider a chain formed by $2N+1$ particles of radius a labeled from $-N$ to N in a coordinate system (X, Y) , the origin of which is centered on the zeroth particle [see Fig. 5(a)]. The magnetic interaction force over the i th particle, and due to the rest of the particles forming the chain, is $\vec{F}_i = F_i^\theta \vec{u}_\theta + F_i^r \vec{u}_r$, with

$$F_i^r = \frac{3\mu_0 m^2}{4\pi} (1 - 3\cos^2\alpha) \left[\sum_{j=-N}^{i-1} \frac{1}{r_{ij}^4} - \sum_{j=i+1}^N \frac{1}{r_{ij}^4} \right], \quad (4.1)$$

$$F_i^\theta = \frac{3\mu_0 m^2}{4\pi} \sin(2\alpha) \sum_{j=-N, j \neq i}^N \frac{1}{r_{ij}^4}, \quad (4.2)$$

where $r_{ij} = |\vec{r}_i - \vec{r}_j| = 2a|i-j|$ is the separation between i th and j th particle centers, and α is the angle between the long axis of the chain and the magnetic field. The mechanical stability of the chain can be determined by an analysis of the radial component of the magnetic force, as was done previously for ER fluids subjected to shear flow [10]. The fragmentation process takes place when the force acting over the N th particle, F_N^r , is repulsive, i.e., $\cos^2\alpha < \sqrt{1/3}$. This condition gives us a critical angle $\alpha_c = 54.7^\circ$, above which the chain will not be stable [20]. In the case of simple shear on ER fluids, the critical angle was found to be $\alpha_c = 39.23^\circ$ because of the different orientation of the hydrodynamic force compared to the present case.

The angular component of the magnetic force will be responsible for the rotation of the chain. The chain orientation is found by balancing the two torques that act on the aggregates. The magnetic torque Γ_m arises because the long axis of the aggregates is not parallel to the single-particle dipole moments, which are aligned parallel to the magnetic field direction. This field-induced torque will be the sum of the torques that are exerted on each particle of the chain,

$$\Gamma_m = 2 \sum_{i=1}^N F_i^\theta r_i, \quad (4.3)$$

where r_i indicates the position of the i th particle. On the other hand, the viscous torque Γ_h is calculated considering the shish-kebab model, where the chain rotates with an angular velocity $(d\alpha/dt - \omega)$ relative to the surrounding liquid,

$$\Gamma_h = \zeta_r \left[\frac{d\alpha}{dt} - \omega \right], \quad (4.4)$$

where

$$\zeta_r = \frac{\pi \eta L^3}{3 \log(L/4a)} \quad (4.5)$$

is the rotational friction factor of the aggregates [21]. Equating these two torques, the equation of motion for the rotating cylinder given by the theorem of kinetic energy is

$$I \frac{d^2\alpha}{dt^2} = \Gamma_h + \Gamma_m, \quad (4.6)$$

where I is the moment of inertia of the rod aggregate. We can typically neglect the inertial term because the viscous drag term dominates. Therefore, after a short transient, α reaches a steady value

$$\sin(2\alpha) = \frac{\pi \eta f L^3}{2\mu_0 a^6 \chi^2 H^2 \log(L/4a) P}, \quad (4.7)$$

where

$$P \equiv \sum_{i=1}^N 2r_i \sum_{j=-N, j \neq i}^N \frac{1}{r_{ij}^4}. \quad (4.8)$$

To simplify the calculation we consider only nearest neighbor interactions to compute $P \approx L^2/2(2a)^5$. Therefore, Eq. (4.7) becomes

$$\sin(2\alpha) = \frac{\pi 2^5 \eta}{\mu_0 a \chi^2} \frac{fL}{H^2 \log(L/4a)}. \quad (4.9)$$

We can rewrite this steady solution as $\sin 2\alpha = f/f_0$ to emphasize that two different regimes occur, as we saw in the experimental results. We can interpret $\tau_0 = 1/f_0$ as the characteristic time of the particle reorganization. A first regime appears for low frequencies ($f < f_0$), where the chain's length remains almost constant (see Fig. 7). This implies that the phase lag increases with frequency, as is deduced from Eq. (4.9). Neglecting in this equation the slow logarithmic dependence, and considering that $\Delta n'' \propto L$, we find the phase lag scaling

$$\sin(2\alpha) \propto \frac{f \Delta n''}{H^2}. \quad (4.10)$$

To examine this scaling we plotted $(\sin 2\alpha)$ vs $(\Delta n'' f)$ in Fig. 10 for $f < f_c$ and for different magnetic field strengths. We find a linear behavior, in agreement with our model, with a slope proportional to H^{-2} . This behavior is shown in a

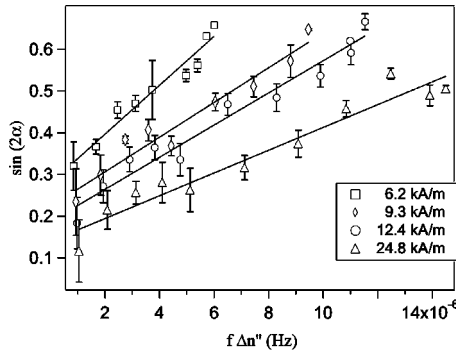


FIG. 10. Plot $\sin(2\alpha)$ vs $(\Delta n'' f)$ to test our theoretical predictions for low frequencies ($f < f_c$) and for different magnetic field intensities.

log-log plot in Fig. 11, where a power law with an exponent $\delta = -2.08 \pm 0.08$ is obtained, following the theoretical prediction.

A second regime appears for high frequencies. In the case of rigid structures, this corresponds to the asynchronous regime, but in our case, the asynchronous regime would lead to phase lag angles larger than α_c , and the chain would not be stable. For that reason, the length chains adapt to approach a synchronous response, and that happens when $f_0(L) \approx f$ is the stable chain. As we observed in experiments, the increase of the phase lag difference is relatively slow (see Fig. 9), and the aggregate size is limited by

$$\frac{L}{\log(L/4a)} \approx \frac{\mu_0 a \chi^2 H^2}{\pi 2^5 \eta f}. \quad (4.11)$$

Neglecting the slow logarithmic dependence in Eq. (4.11), we obtain a scaling $L \propto f^{-1}$, in agreement with the dichroism dependence with frequency $\Delta n'' \propto f^{-1}$ (Fig. 7).

We found in our system that the structures always rotate synchronously with the field because their length can change to decrease the characteristic time of particle reorganization τ_0 . As a result, the domain of synchronous rotation is enlarged compared to the case of solid objects, and a new synchronous regime appears for high frequencies working close to $f_0 \approx f$.

V. CONCLUSIONS

The purpose of this paper was to examine the interplay between the aggregating and orienting effects of magnetic fields on MR fluids, and the influence of hydrodynamic forces. This was accomplished using scattering dichroism to follow the orientation dynamics of field-induced aggregates. This technique allows a determination of both the degree of aggregation and the average angle of orientation relative to a

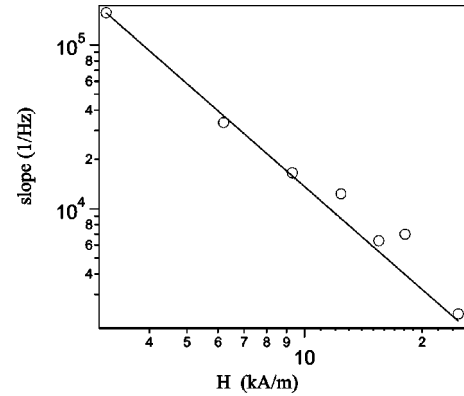


FIG. 11. Power law fit for the slope vs H in a log-log plot leading an exponent $\delta = -2.08 \pm 0.08$.

reference frame. This was applied to both unidirectional and rotating magnetic fields. It is the latter type of field that subjects the aggregates to magnetic forces by causing them to rotate within the suspending fluid and hydrodynamic forces which arise from the rotational friction.

Studies on unidirectional flows establish the utility of the scattering dichroism to study the orientation and relaxation dynamics of MR fluids. As expected, the application of unidirectional magnetic fields induces the formation of fibular aggregates and the appearance of the optical anisotropy of dichroism. Rotating magnetic fields, on the other hand, lead to the addition of hydrodynamic forces that will oppose the orientation of the aggregates. These aggregates are measured to rotate at a phase angle that lags behind the rotating magnetic field. Two different behaviors are found below or above a critical frequency of the magnetic field. For low frequencies the size of the aggregates remains almost constant. Higher frequencies of rotation of the fields are seen to lead to instabilities in the aggregates and to cause fragmentation. So for those frequencies the aggregates' sizes become shorter in order to continue to rotate synchronously with the field. This is observed through a decrease in dichroism at a constant field strength with increasing rotational frequencies. A simple torque balance model predicts this phase angle experimental behavior.

ACKNOWLEDGMENTS

This work was partially supported by the Lai Family Grant. S.M. was supported by the DGICYT (Grant No. PB96-0148). We gratefully acknowledge Oscar G. Calderón for his advice and fruitful discussions, and M.-Carmen Miguel for conversations about diffusion processes. S.M. thanks C. Brooks, E. Wheeler, and D. Olson for helping in the experimental work.

- [1] P.C. Scholten, IEEE Trans. Magn. **MAG-11**, 1400 (1975).
 [2] M. Ferminger and A. Gast, J. Colloid Interface Sci. **154**, 522 (1992).
 [3] D. Wirtz and M. Fermigier, Phys. Rev. Lett. **72**, 2294 (1994).
 [4] E. Lemaire, Y. Grasselli, and G. Bossis, J. Phys. II **2**, 359

- (1992).
 [5] Y.H. Hwang and X-l. Wu, Phys. Rev. E **49**, 3102 (1994).
 [6] H. Zhang and M. Widom, Phys. Rev. E **51**, 2099 (1995).
 [7] J. Liu, E.M. Lawrence, A. Wu, M.L. Ivey, G.A. Flores, K. Javier, J. Bibbette, and J. Richard, Phys. Rev. Lett. **74**, 2828

- (1995).
- [8] A. Silva, R. Bond, F. Plouraboué, and D. Wirtz, *Phys. Rev. E* **54**, 5502 (1996).
- [9] *Proceedings of the 5th International Conference on ER Fluids, MR Suspensions, and Associated Technology*, University of Sheffield, Sheffield, 1995, edited by W. A. Bullough (World Scientific, Singapore, 1996).
- [10] J.E. Martin and R.A. Anderson, *J. Chem. Phys.* **104**, 4814 (1996).
- [11] O. Volkova, S. Cutillas, and G. Bossis, *Phys. Rev. Lett.* **82**, 233 (1999).
- [12] F. Brochard, *J. Phys. (France) Lett.* **35**, 19 (1974).
- [13] D. Lettelier, O. Sandre, C. Menager, V. Cabuil, and M. Lavergne, *Mater. Sci. Eng., C* **5**, 153 (1997).
- [14] O. Sandre, J. Browaeys, R. Perynski, J.-C. Bacri, V. Cabuil, and R.E. Rosensweig, *Phys. Rev. E* **59**, 1736 (1999).
- [15] G. Helgesen, P. Pieranski, and A.T. Skjeltop, *Phys. Rev. Lett.* **64**, 1425 (1990); *Phys. Rev. A* **42**, 7271 (1990).
- [16] Thomas B. Jones, *Electromechanics of Particles* (Cambridge University Press, Cambridge, 1995).
- [17] H.C. van de Hulst, *Light Scattering by Small Particles* (Dover, New York, 1981).
- [18] Gerald G. Fuller, *Optical Rheometry in Complex Fluids* (Oxford University Press, Oxford, 1995).
- [19] Gerald G. Fuller, *Annu. Rev. Fluid Mech.* **22**, 387 (1990).
- [20] J.E. Martin (private communication).
- [21] M. Doi and S.F. Edwards, *The Theory of Polymer Dynamics* (Clarendon Press, Oxford, 1986).